

Photoluminescence and radiative lifetime of trions in GaAs quantum wells

Axel Esser, Erich Runge, and Roland Zimmermann

Institut für Physik, Humboldt-Universität zu Berlin, Hausvogteiplatz 5-7, D-10117 Berlin, Germany

Wolfgang Langbein

Lehrstuhl für Experimentelle Physik E11b, Universität Dortmund, Otto-Hahn-Strasse 4, D-44221 Dortmund, Germany

(Received 15 February 2000)

Electron-trion photoluminescence spectra were measured in undoped high-quality GaAs quantum wells. The obtained line shape depends on temperature and is asymmetric with a tail towards lower photon energies. For a detailed understanding, we have solved numerically the trion Schrödinger equation in the quantum well. Both electron and hole trions are considered. Good agreement is found for the trion binding energy and for the luminescence line shape at different temperatures. The radiative lifetime of thermalized trions is found to increase linearly with temperature. Analytical results are given for both types of trions taking into account the finite photon wave vector (light-cone effect).

I. INTRODUCTION

The three-particle bound state of an exciton with an additional electron (X^- , electron trion) or hole (X^+ , hole trion), as proposed by Lambert,¹ has been observed in bulk materials such as Ge (Ref. 2) by photoluminescence (PL) and Si (Ref. 3) by cyclotron resonance absorption. The experimental signatures of trions are more distinct in semiconductor quantum wells (QW's) because of an enhanced binding energy. The excess carrier density in QW's is usually obtained by (i) doping the barrier material with acceptors or donors,⁴⁻⁶ (ii) by exciting a neighboring thinner QW from which electrons can tunnel more effectively through the barrier than holes,^{7,8} or (iii) by optical excitation in a situation where electrons can escape more easily.⁹ During the past few years, both types of trions (X^- and X^+) have been found in PL and absorption experiments on QW's in III-V compounds as well as in II-VI materials. The specific trion state can be analyzed by means of magneto-optical spectroscopy. In this case, also the triplet states¹⁰ have been observed.

Trion experiments call for samples with large exciton and trion binding energies and small inhomogeneous broadening, which are, however, conflicting goals. The former is realized in thin II-VI systems, whereas the latter is achieved in high-quality GaAs/Al_xGa_{1-x}As QW's. We choose the second variant and present data of a single undoped 25 nm wide QW inbetween Al_{0.3}Ga_{0.7}As barriers. The measured PL exhibits a clearly resolved temperature-dependent asymmetrical peak below the exciton that is attributed to electron trions. We will compare this finding with numerical results obtained from a solution of the three-particle Schrödinger equation. Random spatial fluctuations due to remote ionized donors [case (i)] or interface roughness and alloy disorder¹¹ (all cases) influence particles in real QW's. We minimized these effects by a suitable choice of the sample structure. Consequently, we will be able to describe our experimental findings by delocalized trions, which furthermore are assumed to be in thermodynamic equilibrium.

Earlier theoretical results for the binding energies have been achieved by variational methods for bulk and two-

dimensional (2D) systems by Stébé and co-workers.¹² They also considered the trion absorption coefficient for the ideal 2D and 3D case in Ref. 13. A realistic description has to take into account the effective Coulomb potential due to the carrier confinement and the variation of the dielectric constant from the well to the barrier material. As a qualitative result, we will find below that the QW binding energies of X^- and X^+ are less different than in an ideal 2D case. To our best knowledge the experimental observation of trions in quantum wires and quantum dots is still lacking, although, e.g., quantum wires should exhibit even higher trion binding energies.¹⁴ However, further confinement toward quantum dots brings the carriers closer together, and with an effective increase of the repulsion also a decrease of binding energy could be expected. Variational results by Lelong and Bastard¹⁵ for 0D systems even show negative X^- binding energies in InAs dots.

Another experimentally important property is the radiative lifetime of trions. Several attempts have been made to investigate the trion dynamics. In remotely doped QW's, the trion luminescence shows large spatial fluctuations, that are due to localization in the random potential of the ionized donors.¹⁶ In this case, a radiative lifetime almost independent of temperature is found from resonant trion excitation experiments on GaAs QW's.¹⁷ In contrast, the picture of delocalized trions is more appropriate for the experimental approach on double-QW structures with an optical control of the background free-particle density.¹⁸ Here a linear increase of radiative lifetime and diffusivity with temperature is found. We adopt this assumption of delocalized trions in the present paper and extend the theory for the radiative lifetime of excitons to obtain an analytical expression for the radiative lifetime of thermalized trions.

The outline of this paper is as follows: After a discussion of the experimental setup and results in Sec. II, we present our numerical approach in Sec. III. In particular, the trion binding energy is obtained from the corresponding trion Schrödinger equation. Then, in Sec. IV, the trion wave function is used to study the PL line shape in detail and to com-

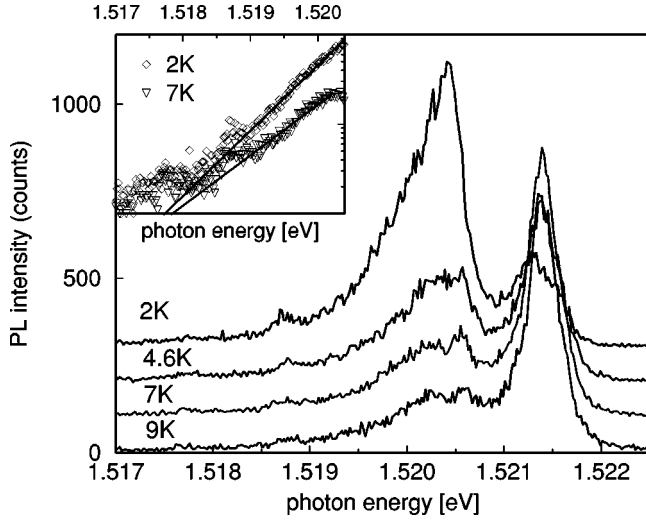


FIG. 1. Trion and exciton photoluminescence spectra of a 25 nm wide GaAs/Al_{0.3}Ga_{0.7}As single QW for different temperatures (vertically displaced for clarity). The excitation is 10 mW/cm² at energy 1.983 eV. The inset shows the experimental low-energy tail of electron trions at 2 K and 7 K, which shows the exponential decay. Note that the peak maximum shifts slightly with higher temperatures.

pare the resulting line shape for electron trions with the experimental data. In Sec. V, we calculate the radiative lifetime of both types of trions including the finite momentum of photons (light-cone effect) and compare the results with the exciton lifetime. We finally summarize our findings in Sec. VI.

II. EXPERIMENTAL DETAILS

The investigated sample is a 25 nm GaAs/Al_{0.3}Ga_{0.7}As QW grown by molecular beam epitaxy on an undoped GaAs substrate. It is placed in a helium cryostat at a temperature between 2 K and 30 K. The sample is excited by a Xe high-pressure lamp spectrally filtered by a monochromator with a resolution of 1 meV. The excitation density on the sample was about 10 mW/cm². The excitation energy was tuned around the barrier band gap in order to control the excess carrier density in the well. Photoluminescence spectra have been dispersed by a double 0.85 m monochromator with a resolution of 0.05 nm (0.1 meV) and detected by a cooled GaAs photomultiplier using photon counting. The large well thickness and the binary well material lead to an interface-roughness- and alloy-disorder-induced linewidth of less than 0.1 meV.¹⁹ The observed exciton linewidth at 2 K and low excess electron density is 0.3 meV in this sample, which allows us to study the trion line shape in detail. The excess electron density in the QW can be controlled by tuning the excitation energy close to the band gap of the barrier, a situation comparable to case (ii). As an example, the PL at a larger excess electron density (excitation at 1.983 eV) and temperatures of 2 K and 7 K are shown in Fig. 1. At 1 meV below the exciton line at $E_X = 1.5214$ eV, the recombination of electron trions shows up as an asymmetric line with a low-energy tail, which broadens with increasing temperature. At this excess density, the exciton linewidth is increased to 0.4 meV, probably due to enhanced exciton-electron scatter-

ing. The small feature at 1.5187 meV is due emission of an impurity-bound exciton, which is also present for low excess carrier densities.

III. TRION SCHRÖDINGER EQUATION

Though the experiment shows electron trions in the PL, we will discuss explicit results for both types of charged excitons. For the sake of simplicity, however, all formulas are given for electron trions X^- . The corresponding formulas for hole trions are obtained by interchanging labels $\{e_1, e_2, h\} \rightarrow \{h_1, h_2, e\}$.

For the calculations, we factorize the wave function of the trion Ψ_T into an in-plane part ψ_T and confinement functions ϕ_e , and ϕ_h of the lowest electron and heavy-hole sublevel, respectively,

$$\Psi_T = \psi_T(\boldsymbol{\rho}_{e1}, \boldsymbol{\rho}_{e2}, \boldsymbol{\rho}_h) \phi_e(z_{e1}) \phi_e(z_{e2}) \phi_h(z_h). \quad (1)$$

The growth direction is along z , and $\boldsymbol{\rho}$ denotes two-dimensional vectors in the QW plane. Strictly speaking, this approximation is only justified in structures where the sublevel distance is large with respect to the exciton binding energy. This is the case in narrow QW's with a Bohr radius exceeding the well width but works reasonably well even in the present case. Furthermore, we separate the center of mass motion (c.m.) of the trion from its relative wave function. The resulting in-plane Schrödinger equation for the latter is ($\mu^{-1} = m_e^{-1} + m_h^{-1}$)

$$\left[-\frac{\hbar^2}{2\mu} (\Delta_{\boldsymbol{\rho}_1} + \Delta_{\boldsymbol{\rho}_2}) - \frac{\hbar^2}{m_h} \nabla_{\boldsymbol{\rho}_1} \cdot \nabla_{\boldsymbol{\rho}_2} - V_{eh}(\boldsymbol{\rho}_1) - V_{eh}(\boldsymbol{\rho}_2) + V_{ee}(|\boldsymbol{\rho}_1 - \boldsymbol{\rho}_2|) - E_T \right] \psi_T(\boldsymbol{\rho}_1, \boldsymbol{\rho}_2) = 0, \quad (2)$$

where relative coordinates $\boldsymbol{\rho}_1 = \boldsymbol{\rho}_{e1} - \boldsymbol{\rho}_h$ and $\boldsymbol{\rho}_2 = \boldsymbol{\rho}_{e2} - \boldsymbol{\rho}_h$ have been introduced. The effective Coulomb potential in Eq. (2)

$$V_{cd}(\boldsymbol{\rho}) = \int \int dz_c dz_d \phi_c^2(z_c) \phi_d^2(z_d) \frac{e^2}{\epsilon_0 \sqrt{\rho^2 + (z_c - z_d)^2}} \quad (3)$$

is slightly different for the electron-electron and electron-hole interaction. This is due to different subband functions ϕ_c for electrons and heavy holes which in turn result from different band offsets and masses. The effective potential (3) has been modified further by image-charge effects, which are due to the different static dielectric constants ϵ_0 in well and barrier materials. The main consequence is an enhancement of all binding energies over the entire range of well widths.²⁰

We numerically solve the trion Schrödinger equation (four spatial degrees of freedom) within a finite-difference scheme by iterating down to the trion singlet ground state.²¹ For the 25 nm GaAs QW, an electron trion binding energy $B_{X^-} = E_X - E_T$ of 0.8 meV is found. The binding energy of the hole trion has been calculated analogously, giving a slightly larger value of $B_{X^+} = 1.0$ meV. These results are in agreement with Ref. 22 where in a comparative study of both types of trions in a 20 nm GaAs QW $B_{X^-} \approx B_{X^+} \approx 1$ meV is found experimentally. For comparison, the exciton Schrö-

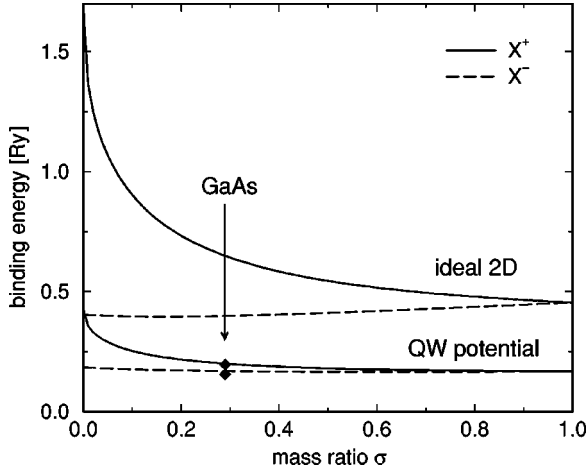


FIG. 2. Binding energies of electron trions (X^-) and hole trions (X^+) as function of mass ratio σ for an ideal 2D Coulomb potential and the effective QW potential, Eq. (4). Symbols correspond to our full analysis for the QW potential including image-charge effects.

ding equation is solved with the same effective potential $V_{eh}(\rho)$ and yields an exciton binding energy of $B_X = 7.8$ meV, in fair agreement with the experimentally deduced value of 7 meV.

Furthermore, we compare these findings with results using the simplified potential

$$V_{cd}(\rho) = \frac{e^2}{\epsilon_0 \sqrt{\rho^2 + (\alpha L_z)^2}}, \quad (4)$$

which avoids the logarithmic singularity in Eq. (3) and has been used for the calculation of binding energies of biexcitons in (Zn,Cd)Se QW's.²¹ In Eq. (4) L_z is the width of the QW, and the parameter α has been used to adjust the exciton energy ($\alpha = 0.17$ in the present case, $L_z = 25$ nm). Using this potential, we have found for the electron trion a binding energy of 0.9 meV and for the hole trion 1.1 meV, which is in good agreement with the results obtained from the more realistic potential, Eq. (3).

As a test for our numerical procedure we have recalculated the trion energies with the ideal 2D Coulomb potential (Fig. 2), which resembles the limit of strong confinement, and found complete agreement with values in the literature.²³ In this limit, the hole-trion binding energy exceeds the electron-trion energy considerably (by a factor of 1.45 at the GaAs mass ratio $m_e/m_h = 0.29$). In contrast, with the realistic effective Coulomb potential, Eq. (3), the hole-trion binding energy is only slightly enhanced. To illustrate these findings, the trion energies using the simplified potential (4) are shown in Fig. 2 as a function of mass ratio $\sigma = m_e/m_h$. Using bulk excitonic units for energy $\text{Ry}^* = \hbar^2 a^{-2}/2\mu$ and length $a = \hbar^2 \epsilon_0 / \mu e^2$ we find that the differences between X^- and X^+ are less distinct in the QW case. If $e-e$ and $e-h$ interaction have equal strength, the trion energies are related by the symmetry relation $E_{X^-}(\sigma) = E_{X^+}(1/\sigma)$. This implies

$$\left. \frac{\partial E_{X^-}}{\partial \sigma} \right|_{\sigma=1} = - \left. \frac{\partial E_{X^+}}{\partial \sigma} \right|_{\sigma=1}, \quad (5)$$

which is fulfilled within our numerical approach. Thus, the comparable binding energies for electron and hole trions in QW's can be attributed to the effective potential (3), which is different from the ideal 2D Coulomb potential in particular at the origin. As can be checked by the agreement with the full potential calculation (symbols in Fig. 2), the minor difference between attractive and repulsive potential is of no importance.²²

IV. PHOTOLUMINESCENCE

Using the calculated trion wave function, we study the optical transition from a delocalized trion to an unpaired electron in the conduction band. Using Fermi's golden rule, the main ingredient of the optical matrix element (derived in detail below) when neglecting the photon momentum is

$$M(\mathbf{Q}) = \int d\boldsymbol{\rho}_2 \psi_{X^-}(0, \boldsymbol{\rho}_2) \exp(-i\mathbf{Q} \cdot \boldsymbol{\rho}_2 M_X / M_T), \quad (6)$$

where the trion at total momentum \mathbf{Q} decays radiatively, leaving an electron with the same momentum behind. Here, $M_X = m_e + m_h$ is the exciton mass, and $M_T = 2m_e + m_h$ the electron-trion mass. Expression (6) is identical to the optical matrix element which was obtained by Stébé *et al.*¹³ for the trion-related absorption at $T = 0$ K. It can be regarded as a generalization of the excitonic transition rate for trions (one relative coordinate is set to zero). Assuming in the low-density regime a thermal Boltzmann distribution of trions with energy $E_T + \hbar^2 Q^2 / 2M_T$, the PL line shape is given by

$$\begin{aligned} P_T(\hbar\omega) &= \int d\mathbf{Q} \exp\left(-\frac{\hbar^2 Q^2}{2M_T k_B T}\right) |M(\mathbf{Q})|^2 \\ &\times \delta\left(\hbar\omega - E_T + \frac{\hbar^2 Q^2}{2m_e} \frac{M_X}{M_T}\right) \\ &\propto |M(\mathbf{Q})|^2 \exp\left(-\frac{\epsilon}{k_B T} \frac{m_e}{M_X}\right) \Theta(\epsilon). \end{aligned} \quad (7)$$

The energy-conserving δ function in Eq. (7) determines the momentum as a function of photon energy via

$$\epsilon = E_T - \hbar\omega = \frac{\hbar^2 Q^2}{2m_e} \frac{M_X}{M_T}. \quad (8)$$

A material-dependent prefactor (containing trion density and temperature) is omitted, but taken care of later when calculating the radiative rate. The PL line has a sharp onset at the trion energy, followed towards lower photon energies by a temperature-dependent tail that is due to the recombination of thermally excited trions with $Q > 0$ leaving a recoil electron behind. For electron trions, the wave function $\psi_T(0, \boldsymbol{\rho}_2)$ entering Eq. (6) is close to a Gauss shape, and the optical matrix element can be well approximated by $|M(\mathbf{Q})|^2 = c_1 e^{-\epsilon/\epsilon_1}$ with $\epsilon_1 = 1.1$ meV and $c_1 = 15.0$. The temperature dependence of the electron-trion emission, which we obtain from our numerics, is shown in Fig. 3 and follows an exponential decay on the low-energy side. This exponential behavior is found for the experimental trion line as well, as can be seen in the inset of Fig. 1, where the low-energy tail

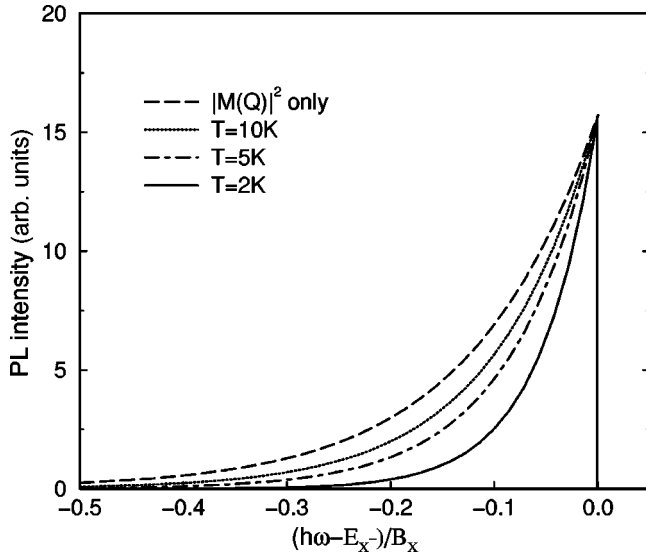


FIG. 3. Calculated temperature dependence of the electron-trion emission line shape. Energies are scaled with the QW exciton binding energy B_x . In the high-temperature limit, the line shape is directly given by $|M(Q)|^2$.

of the electron trion is displayed on a logarithmic scale. The deviations at very low energies are due to background contributions.

In the case of hole trions (Fig. 4), the calculated line shape is again rather smooth. In comparison with electron trions, it falls off more rapidly because of the larger hole-trion mass. Due to the more effective hole-hole repulsion at short distances, a slightly nonexponential shape is found. Neglecting this small deviation, the optical matrix element decays in this case exponentially with $\epsilon_1 = 0.5$ meV and $c_1 = 12.8$.

In Fig. 5, we compare the full experimental data of Fig. 1 at 2 K and 7 K with our numerical findings. The broadened

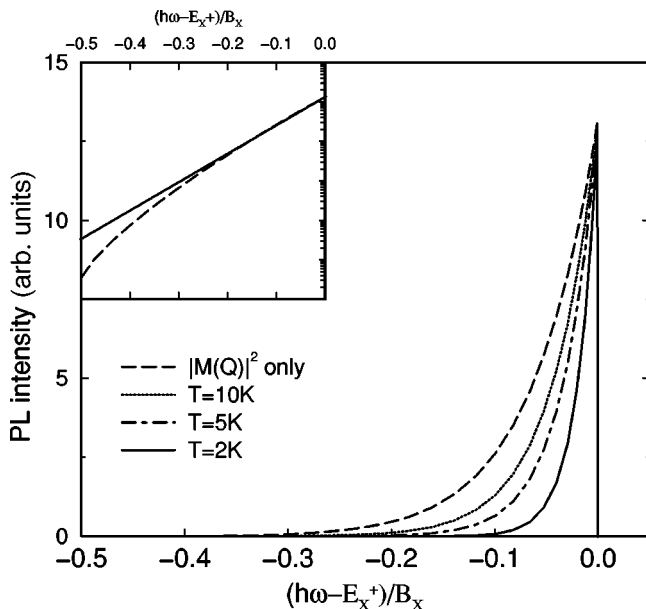


FIG. 4. Calculated temperature dependence of the hole-trion line shape on linear and logarithmic (inset) scale. A slight nonexponential decay is found as a result of the more effective hole-hole repulsion at short distances.

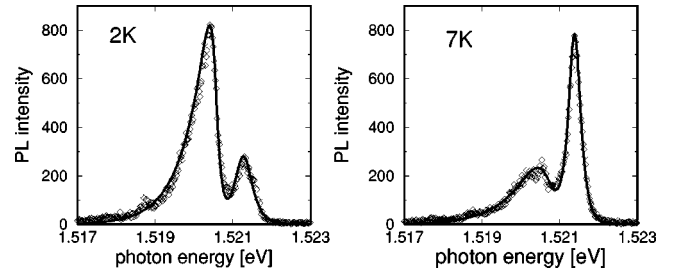


FIG. 5. Trion and exciton photoluminescence of a 25 nm wide GaAs/Al_{0.3}Ga_{0.7}As single QW at different temperatures. Comparison between experiment (symbols) and calculated spectra. (The overall ratio between exciton and trion peak has been fitted.)

exciton line is well fitted with a hyperbolic secant profile, which is related to the exponential tail in phonon scattering. Then, the trion contribution is found from the convolution of Eq. (7) with the same profile. Depending on the derived exciton width [full width at half maximum (FWHM) = 0.5 meV at 2 K, and 0.4 meV at 7 K], the convolution shifts the trion peak maximum toward slightly lower energies (here ≈ 0.1 meV). Thus, in the experimental determination of the trion binding energy the inflection point on the high-energy shoulder is a better choice instead of using the peak position.

The reasonable agreement of the experimental trion PL line shape with our calculations in Fig. 5 leads to the conclusion that thermalization at least within the trion population can be expected. Complete thermal equilibrium between trions and excitons has been found in Refs. 8 and 18 using a double-QW sample. In contrast to modulation doping this allows an optical control of the excess electron density. To quantify the relative weight of exciton and trion PL, we have studied an equilibrium mass action law between excitons, trions, free electrons, and free holes.²⁹ This allows to discuss the dependence of the emission on temperature, background density, and excitation density. Since the low-energy tail of each trion PL could be well fitted using the nominal lattice temperature, a significantly elevated effective temperature of the trions can be ruled out.

V. RADIATIVE LIFETIME OF THERMALIZED TRIONS

A. Interaction Hamiltonian

In order to compare the radiative lifetime of thermalized excitons and trions we will calculate both values on an equal footing. For the exciton, the lifetime was calculated already by Andreani *et al.* in Ref. 24 with a later correction of an erroneous factor of 2; see Ref. 25. Unfortunately, in Ref. 26 experimental results have been compared with the earlier version. To circumvent such kinds of problems for trions and to illustrate the algebra needed for the trion calculation, we want to recalculate the correct result of Andreani *et al.* The first step is the derivation of the light-matter interaction Hamiltonian taking into account the specific structure of the valence band edge in GaAs.

The electromagnetic field enters the kinetic part of the Hamiltonian via the vector potential $\mathbf{A}(\mathbf{r})$:

$$H_{\text{kin}} = \sum_s \int d\mathbf{r} \hat{\psi}_s^\dagger(\mathbf{r}) \frac{1}{2m_0} \left[\hat{\mathbf{p}} - \frac{e}{c} \mathbf{A}(\mathbf{r}) \right]^2 \hat{\psi}_s(\mathbf{r}). \quad (9)$$

The spin-dependent electron field operators $\hat{\psi}_s(\mathbf{r})$ are expanded into localized Wannier functions u_ν according to

$$\hat{\psi}_s(\mathbf{r}) = \sum_{\mathbf{R}\nu} c_{\mathbf{R}\nu} u_\nu(\mathbf{r} - \mathbf{R}, s), \quad (10)$$

where $c_{\mathbf{R},\nu}$ annihilates an electron at lattice vector \mathbf{R} in band ν . Under low-density excitation, we restrict ourselves to the linear regime. Using the Coulomb gauge ($\nabla \cdot \mathbf{A} = 0$) the light-matter interaction reduces to

$$H_{\text{rad}} = \frac{e}{cm_0} \sum_{\mathbf{R}\nu\nu'} \mathbf{A}(\mathbf{R}) c_{\mathbf{R}\nu}^\dagger c_{\mathbf{R}\nu'} \sum_s \int d\mathbf{r} u_\nu^*(\mathbf{r}, s) \hat{\mathbf{p}} u_{\nu'}(\mathbf{r}, s), \quad (11)$$

where we assume the Wannier functions to have no overlap at different lattice sites, and the vector potential $\mathbf{A}(\mathbf{r})$ to be a slowly varying function within an elementary cell. Now, we identify the Wannier functions u_ν with spin-orbit coupled atomiclike functions for heavy holes,

$$\left| \frac{3}{2}, \frac{3}{2}, \sigma \right\rangle = \frac{1}{\sqrt{2}} |X + i\sigma Y\rangle \left| \frac{1}{2}, \sigma \right\rangle \quad (12)$$

in the valence band v , and for electrons,

$$\left| \frac{1}{2}, \frac{1}{2}, \sigma \right\rangle = |S\rangle \left| \frac{1}{2}, \sigma \right\rangle \quad (13)$$

in the conduction band c . In this representation, the spin index attains the values $\sigma = \pm 1$. Within the rotating-wave approximation, Eq. (11) takes the form

$$H_{\text{rad}} = \frac{e}{cm_0} \frac{p_{cv}}{\sqrt{2}} \sum_{\mathbf{R}\sigma} [A_x(\mathbf{R}) + i\sigma A_y(\mathbf{R})] c_{\mathbf{R}v\sigma}^\dagger c_{\mathbf{R}c\sigma} + \text{H.c.}, \quad (14)$$

with the momentum matrix element $p_{cv} = \langle X | p_x | S \rangle$. The vector potential $\mathbf{A}(\mathbf{r})$ is expanded into plane-wave eigenmodes within a normalization volume Ω according to²⁷

$$\mathbf{A}(\mathbf{r}) = \sum_{\mathbf{q}\lambda} \sqrt{\frac{2\pi\hbar c}{nq\Omega}} \mathbf{e}_{\mathbf{q}\lambda} (a_{\mathbf{q}\lambda} e^{i\mathbf{q}\cdot\mathbf{r}} + a_{\mathbf{q}\lambda}^\dagger e^{-i\mathbf{q}\cdot\mathbf{r}}). \quad (15)$$

Here, $a_{\mathbf{q}\lambda}^\dagger$ creates a photon with wave vector \mathbf{q} and polarization λ in the QW material with refractive index $n = \sqrt{\epsilon_0}$. Then, by converting the lattice sum into an integral, the interaction Hamiltonian is found as

$$H_{\text{rad}} = \frac{ep_{cv}}{cm_0} \sum_{\sigma} \sum_{\mathbf{q}\lambda} \sqrt{\frac{\pi\hbar c}{nq\Omega}} [e_{\lambda,x} + i\sigma e_{\lambda,y}] a_{\mathbf{q}\lambda}^\dagger \times \int d\mathbf{r} c_{v\sigma}^\dagger(\mathbf{r}) c_{c\sigma}(\mathbf{r}) e^{-i\mathbf{q}\cdot\mathbf{r}} + \text{H.c.} \quad (16)$$

Using polar coordinates along the growth direction, the two transversal photon polarizations can be chosen as $\mathbf{e}_{\lambda=1} = (-\sin\phi, \cos\phi, 0)$ and $\mathbf{e}_{\lambda=2} = (-\cos\theta\cos\phi, -\cos\theta\sin\phi, \sin\theta)$, which results for the in-plane components in

$$e_{\lambda,x} + i\sigma e_{\lambda,y} = \begin{cases} i\sigma e^{i\sigma\phi}, & \lambda=1 \\ -\cos\theta e^{i\sigma\phi}, & \lambda=2. \end{cases} \quad (17)$$

Equation (16) will be used in the following calculation of both the radiative lifetime of excitons and trions.

B. Exciton lifetime

The radiative lifetime of excitons τ_X is found from Fermi's golden rule as

$$\tau_X^{-1} = \frac{2\pi}{\hbar} \sum_{if} | \langle f | H_{\text{rad}} | i \rangle |^2 \delta(\epsilon_i - \epsilon_f) N_i. \quad (18)$$

N_i denotes the occupation of the exciton in the initial states, normalized to unit total density, $\sum_i N_i = 1$. The main ingredient is the optical matrix element between the initial exciton state at c.m. vector \mathbf{Q}

$$|i\rangle = \int d\mathbf{r}_e \int d\mathbf{r}_h \frac{e^{i\mathbf{Q}\cdot\mathbf{R}}}{\sqrt{\mathcal{A}}} \Phi_X(\boldsymbol{\rho}_e - \boldsymbol{\rho}_h) \phi_e(z_e) \phi_h(z_h) \times c_{c\sigma}^\dagger(\mathbf{r}_e) c_{v\sigma}(\mathbf{r}_h) |0\rangle, \quad (19)$$

(\mathcal{A} is the normalization area) and the final photon state $|f\rangle = a_{\mathbf{q}\lambda}^\dagger |0\rangle$. The crystal ground state $|0\rangle$ at $T=0$ K describes the full valence band, the empty conduction band, and photon vacuum. Decomposing the photon wave vector as $\mathbf{q} = \{\mathbf{q}_{\parallel}, q_z\}$ and using Eq. (16), the optical matrix element is given by

$$\langle f | H_{\text{rad}} | i \rangle = \frac{e\hbar p_{cv}}{m_0 n} \sqrt{\frac{\pi\mathcal{A}}{E_X \Omega}} \Phi_X(0) [e_{\lambda,x} + i\sigma e_{\lambda,y}] I(q_z) \delta_{\mathbf{Q}, \mathbf{q}_{\parallel}}. \quad (20)$$

The overlap of the confinement functions $I(q_z) = \int dz \phi_e(z) \phi_h(z) e^{-iq_z z}$ can be approximated in the strong confinement limit by unity. The summation over q_z in Eq. (18) yields the one-dimensional density of states for radiative decay. In contrast to bulk semiconductors, where the conservation of the exciton wave vector leads to stationary modes (polaritons), which do not radiatively recombine, this density gives rise to recombination of QW excitons with a wave vector inside the light cone $Q \leq q_0$, given by the photon dispersion $q_0 = nE_X/\hbar c$.²⁵ Explicitly, we have

$$\tau_X^{-1} = \frac{S_0 q_0 \Phi_X^2(0)}{\mathcal{A}} \sum_{\lambda} \sum_{\sigma} |e_{\lambda,x} + i\sigma e_{\lambda,y}|^2 \frac{\Theta(q_0 - Q)}{\sqrt{q_0^2 - Q^2}} N_{X,Q} \\ = \frac{S_0 \Phi_X^2(0)}{\mathcal{A}} g_X^{\text{rad}} \sum_{\sigma} \left(\frac{1}{\sqrt{1 - (Q/q_0)^2}} + \sqrt{1 - (Q/q_0)^2} \right) \times N_{X,Q} \Theta(q_0 - Q), \quad (21)$$

with $S_0 = 2\pi e^2 p_{cv}^2 / m_0^2 c^2 \hbar q_0$. Here, the sum over $\sigma = \pm 1$ gives rise to $g_X^{\text{rad}} = 2$, the number of optically allowed exciton states. For GaAs, we take Kane's matrix element as $2p_{cv}^2/m_0 = 22.7$ eV.³⁰ The two contributions in Eq. (21) result from the two photon polarizations λ (note the extra $\cos\theta$ for $\lambda=2$). We want to emphasize that no assumption about the orientation of the in-plane exciton wave vector \mathbf{Q} has to be made. We consider a completely thermalized exciton distribution $N_{X,Q} = (2\pi\hbar^2/g_X M_X k_B T) \exp(-\hbar^2 Q^2/2M_X k_B T)$, where g_X denotes the number of degenerate and occupied

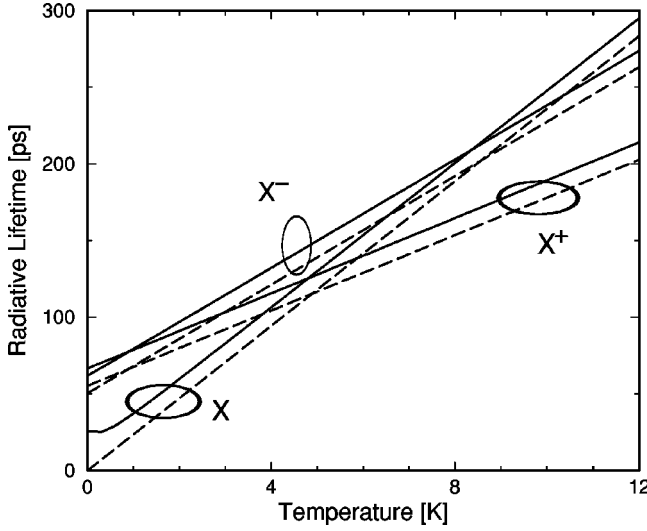


FIG. 6. Calculated radiative lifetime of excitons (X), electron trions (X^-), and hole trions (X^+). Full curves correspond to a complete analysis of the light-cone effect; dashed lines neglect the finite photon momentum.

exciton states. Thus after rapid spin relaxation between bright and dark states, $g_X=4$, and Eq. (21) can be cast into

$$\tau_X = 2\tau_{0,X}H\left[\frac{k_B T}{E_0}\right]. \quad (22)$$

Here, $E_0 = \hbar^2 q_0^2 / 2M_X = 0.07$ meV is the exciton kinetic energy on the light cone, and the auxiliary function $H(y)$ is defined in the Appendix. The temperature-independent prefactor $\tau_{0,X} = 1/S_0 \Phi_X^2(0)$ is the lifetime of a bright-state exciton at $Q=0$ and agrees with the value in the work of Andreani *et al.*²⁵ [note that $H(0)=1$]. With increasing temperature, a diminishing fraction of the exciton distribution is inside the light cone and is able to decay radiatively. Taking the high-temperature limit of this expression [see Eq. (A5)] the radiative lifetime of thermalized excitons is found to change linearly with temperature,

$$\tau_X = \frac{3\tau_{0,X}}{2E_0} \left(k_B T + \frac{3}{5} E_0 \right). \quad (23)$$

The full numerical evaluation of Eq. (22) is presented in Fig. 6 and shows a subtle deviation from Eq. (23) at very low temperatures. Starting with $2\tau_{0,X}$ at $T=0$ K, it exhibits a small (parabolic) decrease before merging to the limiting behavior of Eq. (23) at elevated temperatures.

We remark that in real QW structures excitons are localized by an effective c.m. potential, which results from averaging the exciton relative wave function over the microscopic disorder landscape. Then a thermalized exciton distribution cannot be expected at low temperatures. Numerical simulations of the relaxation kinetics resulted in a non-equilibrium distribution, and significant deviations from Eq. (23) are found.²⁸ In particular, the exciton lifetime is almost independent of temperature at $k_B T < \sigma$, where σ is the variance of the disorder potential. At elevated temperatures lo-

calization effects are of minor importance, and the linear increase of lifetime prevails, as found experimentally; see, e.g., Ref. 26.

C. Trion lifetime

In calculating the recombination rates for trions, we closely follow the exciton case described before. Adopting the separation of c.m. and relative coordinates according to Sec. IV, the initial trion singlet state, where the electron spin part of the trion wave function is antisymmetric ($\sigma_{e_1} = \uparrow$ and $\sigma_{e_2} = \downarrow$), is written as

$$|i\rangle = \int d\mathbf{r}_{e_1} \int d\mathbf{r}_{e_2} \int d\mathbf{r}_h \frac{e^{i\mathbf{Q}\cdot\mathbf{R}}}{\sqrt{A}} \psi_T(\boldsymbol{\rho}_{e_1} - \boldsymbol{\rho}_h, \boldsymbol{\rho}_{e_2} - \boldsymbol{\rho}_h) \\ \times \phi_e(z_{e_1}) \phi_e(z_{e_2}) \phi_h(z_h) c_{c,\uparrow}^\dagger(\mathbf{r}_{e_1}) c_{c,\downarrow}^\dagger(\mathbf{r}_{e_2}) c_{v,\sigma_h}(\mathbf{r}_h) |0\rangle. \quad (24)$$

According to the two possible spin orientations of the heavy hole, two trion states are possible ($\sigma_h = \pm 1$), which both are dipole allowed and can decay radiatively. After the recombination process, an unpaired electron with wave vector \mathbf{k} and spin σ_e and a photon with wave vector \mathbf{q} and polarization λ is left as the final state:

$$|f\rangle = \int d\mathbf{r}_e \frac{e^{i\mathbf{k}\cdot\boldsymbol{\rho}_e}}{\sqrt{A}} \phi_e(z_e) c_{c\sigma_e}^\dagger(\mathbf{r}_e) a_{\mathbf{q}\lambda}^\dagger |0\rangle. \quad (25)$$

The optical matrix element between these states for the interaction Hamiltonian (16) is

$$\langle f | H_{\text{rad}} | i \rangle = \frac{e p_{cv} \hbar}{m_0 n} \sqrt{\frac{\pi A}{E_T \Omega}} [e_{\lambda,x} + i \sigma_e e_{\lambda,y}] \\ \times (\delta_{\sigma_e, \downarrow} \delta_{\sigma_h, \uparrow} - \delta_{\sigma_h, \uparrow} \delta_{\sigma_e, \downarrow}) \\ \times \int d\boldsymbol{\rho} e^{i[(m_e/M_T)\mathbf{Q} - \mathbf{k}] \cdot \boldsymbol{\rho}} \psi_T(0, \boldsymbol{\rho}) \delta_{\mathbf{Q}, \mathbf{k} + \mathbf{q}_{\parallel}}. \quad (26)$$

The integral can be written as matrix element $M[\mathbf{Q} - (M_T/M_X)\mathbf{q}_{\parallel}]$ and improves over Eq. (6) by including the finite in-plane photon momentum \mathbf{q}_{\parallel} . Then, applying Fermi's rule the radiative lifetime is found from

$$\tau_T^{-1} = \frac{S_0}{A^2} g_T^{\text{rad}} \sum_{\mathbf{Q}_{\parallel}} \left(\frac{1}{\sqrt{1 - (q_{\parallel}/q_0)^2}} + \sqrt{1 - (q_{\parallel}/q_0)^2} \right) \\ \times \left| M \left(\mathbf{Q} - \frac{M_T}{M_X} \mathbf{q}_{\parallel} \right) \right|^2 N_{T,Q} \Theta(q_0 - q_{\parallel}). \quad (27)$$

The assumption of a (normalized) thermalized trion distribution

$$N_{T,Q} = \frac{2\pi \hbar^2}{g_T M_T k_B T} \exp\left(-\frac{\hbar^2 Q^2}{2M_T k_B T}\right) \quad (28)$$

has been successfully applied for describing the PL line shape at different temperatures. Here, the number of singlet trion states g_T is equal to the number of optical allowed trions $g_T = g_T^{\text{rad}} = 2$. Adopting the exponential fit of the matrix element given in Sec. IV, Eq. (27) yields the remarkably simple result similar to Eq. (22),

$$\tau_T = \tau_{0,T} H \left[\frac{M_X}{M_T} \left(\frac{k_B T}{E_0} + \frac{\epsilon_1 m_e}{E_0 M_X} \right) \right], \quad (29)$$

with a temperature-independent lifetime $\tau_{0,T} = 2\pi\hbar^2 M_T / S_0 m_e \epsilon_1 c_1 M_X$. The high-temperature limit is found as before using Eq. (A5),

$$\tau_T = \frac{3M_X \tau_{0,T}}{4M_T E_0} \left(k_B T + \epsilon_1 \frac{m_e}{M_X} + \frac{3}{5} \frac{M_T}{M_X} E_0 \right). \quad (30)$$

In contrast to excitons, where the recombination process is restricted to the light cone, trions with arbitrary $Q \geq 0$ can decay radiatively. This is contained in the matrix element $M(\mathbf{Q})$ and introduces an additional offset at zero temperature [second term in Eq. (30)]. The third term is the direct consequence of the inclusion of the finite photon wave vector. The ratio R_- between the temperature slopes of the lifetime for electron trions (30) and excitons (23) is

$$R_- = \frac{\pi\hbar^2 \Phi_X^2(0)}{m_e \epsilon_1 c_1} = \frac{1}{2} \frac{M_X}{M_T} \frac{\Phi_X^2(0)}{\int d\boldsymbol{\rho} |\psi_T(0, \boldsymbol{\rho})|^2}. \quad (31)$$

The second equality gives the ratio in terms of the corresponding exciton and trion wave functions (and was used as a numerical test for the exponential fit of the matrix element in Sec. IV). The numerical value of $R_- \approx 0.75$ for electron trions is determined by the mass ratio and the factor $g_X^{\text{rad}}/g_X = 1/2$, which accounts for dark excitons in spin-equilibrated systems. The integral over the trion wave function can be visualized as probability distribution of the second electron under the condition that the first one is exactly at the hole position. Approaching the electron-hole pair ($\rho \rightarrow 0$), the second electron repels the first electron, and a drastic decrease of the trion transition probability is found.

The same analysis was repeated for the lifetime of hole trions. The ratio of temperature slopes between hole trions and excitons is found from our numerical treatment as $R_+ \approx 0.52$ (here $M_T = 2m_h + m_e$). The radiative lifetime of thermalized electron and hole trions is shown in Fig. 6 as a function of temperature. Due to the contribution of the recombination channel with $Q > 0$, the offset at zero temperatures yields a considerably higher lifetime in comparison with the exciton. Only at elevated temperatures, does the exciton lifetime exceed the trion one. In contrast to excitons, where the full numerical treatment of the light-cone effect exhibits a slight initial decrease at very small temperatures, for trions the expansion (30) is a very good approximation for any temperature.

VI. CONCLUSIONS

In conclusion, our numerically calculated electron-trion wave function leads to photoluminescence spectra that are in

sound agreement with experimental data from a high-quality single GaAs QW. In particular, we found both experimentally and from the numerics that the electron-trion line shape decays exponentially on the low-energy side. A Boltzmann distribution has been used to model the temperature dependence of the PL in this low-density excitation experiment. The radiative lifetimes of thermalized excitons and trions increase linearly with temperature. The recombination processes of trions with a finite in-plane momentum outside the radiative cone create a low-energy tail of the trion PL and lead to a finite lifetime at zero temperatures. Including the finite photon wave vector (light-cone effect) shifts all lifetimes to slightly higher values, with a peculiarity at low temperatures for the exciton only.

The linear increase of trion lifetime with temperature has been observed in QW structures, where the excess density is achieved by exciting a neighboring QW,¹⁸ or in doped samples, where the influence of the random position of the ionized donors/acceptors is reduced significantly. A quantitative comparison with calculations is deferred to a subsequent publication.

ACKNOWLEDGMENTS

We acknowledge helpful discussions with B. Deveaud, S. Haacke, V. Ciulin, P. Kossacki, P. Selbmann, and V. Savona. Financial support by the DFG within the frame of SFB 296 is gratefully acknowledged.

APPENDIX A: LIGHT-CONE FUNCTION

The auxiliary function in Eq. (22) is defined as

$$\frac{1}{H(y)} = \frac{1}{2y} \int_0^1 dx \left(\sqrt{1-x} + \frac{1}{\sqrt{1-x}} \right) e^{-x/y}, \quad (A1)$$

where the integration variable is $x = (Q/q_0)^2$. The prefactor is chosen to give $H(0) = 1$. In order to find the high-temperature expansion (e.g., $y \rightarrow \infty$), we transform the integral into

$$\frac{1}{H(y)} = \int_0^{1/\sqrt{y}} \frac{ds}{\sqrt{y}} (ys^2 + 1) e^{s^2} e^{-1/y}. \quad (A2)$$

With the definition of Dawson's integral $F(x) = e^{-x^2} \int_0^x dt e^{t^2}$, we find

$$\frac{1}{H(y)} = \frac{1}{2} + \frac{2-y}{2\sqrt{2}} F\left(\frac{1}{\sqrt{y}}\right). \quad (A3)$$

Then, using the expansion

$$F(x) = x - \frac{2}{3}x^3 + O(x^5), \quad (A4)$$

we get the expansion valid at large arguments y

$$H(y) \Rightarrow \frac{3}{4} \left(y + \frac{3}{5} \right). \quad (A5)$$

- ¹M.A. Lampert, Phys. Rev. Lett. **1**, 450 (1958).
- ²G.A. Thomas and T.M. Rice, Solid State Commun. **23**, 359 (1977).
- ³T. Kawabata, K. Muro, and S. Narita, Solid State Commun. **23**, 267 (1977).
- ⁴K. Kheng, R.T. Cox, Y. Merle d'Aubigné, F. Bassani, K. Saminadayar, and S. Tatarenko, Phys. Rev. Lett. **71**, 1752 (1993).
- ⁵A.J. Shields, J.L. Osborne, M.Y. Simmons, M. Pepper, and D.A. Ritchie, Phys. Rev. B **52**, R5523 (1995).
- ⁶V. Huard, R.T. Cox, K. Saminadayar, A. Arnoult, and S. Tatarenko, Phys. Rev. Lett. **84**, 187 (2000).
- ⁷A. Manassen, E. Cohen, A. Ron, E. Linder, and L.N. Pfeiffer, Phys. Rev. B **54**, 10 609 (1996).
- ⁸J. Siviniant, D. Scalbert, A.V. Kavokin, D. Coquillat, and J.-P. Lascaray, Phys. Rev. B **59**, 1602 (1999).
- ⁹J.L. Osborne, A.J. Shields, M. Pepper, F.M. Bolton, and D.A. Ritchie, Phys. Rev. B **53**, 13 002 (1996).
- ¹⁰A.J. Shields, J.L. Osborne, M.Y. Simmons, M. Pepper, and D.A. Ritchie, Phys. Rev. B **52**, R5523 (1995).
- ¹¹E. Runge and R. Zimmermann, Phys. Status Solidi A **164**, 511 (1997).
- ¹²B. Stébé and G. Munchy, Solid State Commun. **17**, 1051 (1975); B. Stébé, G. Munsch, L. Stauffer, F. Dujardin, and J. Murat, Phys. Rev. B **56**, 12 454 (1997).
- ¹³B. Stébé, E. Feddi, A. Ainane, and F. Dujardin, Phys. Rev. B **58**, 9926 (1998).
- ¹⁴P. Selbmann (unpublished).
- ¹⁵Ph. Lelong and G. Bastard, Solid State Commun. **98**, 819 (1996).
- ¹⁶G. Finkelstein, H. Shtrikman, and I. Bar-Joseph, Phys. Rev. Lett. **74**, 976 (1995); G. Eytan, Y. Yayon, M. Rappaport, H. Shtrikman, and I. Bar-Joseph, *ibid.* **81**, 1666 (1998).
- ¹⁷G. Finkelstein, V. Umansky, I. Bar-Joseph, V. Ciulin, S. Haacke, J.-D. Garnière, and B. Deveaud, Phys. Rev. B **58**, 12 637 (1998).
- ¹⁸A. Ron, H.W. Yoon, M.D. Sturge, A. Manassen, E. Cohen, and L.N. Pfeiffer, Solid State Commun. **97**, 741 (1996); H.W. Yoon, A. Ron, M.D. Sturge, and L.N. Pfeiffer, *ibid.* **100**, 743 (1996).
- ¹⁹W. Langbein and J.M. Hvam, Phys. Rev. B **61**, 1692 (2000).
- ²⁰D.B. Tran Thoai, R. Zimmermann, M. Grundmann, and D. Bimberg, Phys. Rev. B **42**, 5906 (1990).
- ²¹O. Mayrock, H.-J. Wünsche, F. Henneberger, C. Riva, V.A. Schweigert, and F.M. Peeters, Phys. Rev. B **60**, 5582 (1999).
- ²²S. Glasberg, G. Finkelstein, H. Shtrikman, and I. Bar-Joseph, Phys. Rev. B **59**, R10 425 (1999).
- ²³J. Usukura, Y. Suzuki, and K. Varga, Phys. Rev. B **59**, 5652 (1999).
- ²⁴L.C. Andreani, F. Tassone, and F. Bassani, Solid State Commun. **77**, 641 (1991).
- ²⁵L. C. Andreani, in *Confined Electrons and Photons*, edited by E. Burstein and C. Weisbuch (Plenum Press, New York, 1995), pp 57–112.
- ²⁶M. Colocci, M. Gurioli, and J. Martinez-Pastor, J. Phys. IV **3**, 3 (1993).
- ²⁷H. Haug and S. Koch, *Quantum Theory of the Optical and Electronic Properties of Semiconductors* (World Scientific, Singapore, 1994).
- ²⁸R. Zimmermann, E. Runge, and F. Grosse, in *Proceedings of the 23rd International Conference on the Physics of Semiconductors, Berlin, Germany, 1996*, edited by M. Scheffler and R. Zimmermann (World Scientific, Singapore, 1996), pp. 1935–1942.
- ²⁹A. Esser, E. Runge, R. Zimmermann, and W. Langbein, Phys. Status Solidi A **178**, 489 (2000).
- ³⁰G. Bastard, *Wave Mechanics Applied to Semiconductor Heterostructures* (Les éditions de la physique, Paris, 1988).